APPLIED SCIENCES AND ENGINEERING

High-strength and fibrous capsule–resistant zwitterionic elastomers

Dianyu Dong[1,2]*, Caroline Tsao[1]*, Hsiang-Chieh Hung[1]*, Fanglian Yao[2], Chenjue Tang[1], Liqian Niu[1], Jinrong Ma[1], Joel MacArthur[1], Andrew Sinclair[1], Kan Wu[1], Priyesh Jain[1], Mitchell Ryan Hansen[1], Dorathy Ly[1], Sebastian Gia-huy Tang[1], Tammy My Luu[1], Parul Jain[1], Shaoyi Jiang[1,3†]

The high mechanical strength and long-term resistance to the fibrous capsule formation are two major challenges for implantable materials. Unfortunately, these two distinct properties do not come together and instead compromise each other. Here, we report a unique class of materials by integrating two weak zwitterionic hydrogels into an elastomer-like high-strength pure zwitterionic hydrogel via a "swelling" and "locking" mechanism. These zwitterionic-elastomeric-networked (ZEN) hydrogels are further shown to efficaciously resist the fibrous capsule formation upon implantation in mice for up to 1 year. Such materials with both high mechanical properties and long-term fibrous capsule resistance have never been achieved before. This work not only demonstrates a class of durable and fibrous capsule–resistant materials but also provides design principles for zwitterionic elastomeric hydrogels.

INTRODUCTION

Synthetic hydrogels have long been attractive materials to mimic biological tissues for medical applications such as tissue scaffolding (*1*–*5*). There are two main criteria for achieving this goal: excellent mechanical properties and long-term resistance to the fibrous capsule formation induced by the foreign body reaction. However, these properties generally do not coexist in the same material and compromise each other, as the former requires hydrophobicity while the latter requires hydrophilicity (*6*, *7*). While in vitro protein adsorption, cell adhesion, and cytotoxicity are commonly used to evaluate biomaterials, they are far from the challenges involving fibrous capsule resistance in complex living systems. The ability of the material not to trigger the fibrous capsule formation after implantation for a long period is particularly challenging. It is well known that nearly all synthetic materials trigger the foreign body reaction and fibrous capsule formation within 1 month upon materials implantation (*8*–*11*). While many efforts have been made to mitigate this foreign body reaction through materials geometry or chemical modification (*5*, *12*), super-hydrophilic zwitterionic hydrogels are particularly promising for solving this issue (*6*, *8*, *9*, *13*–*20*). In our early studies, zwitterionic poly(carboxybetaine) (pCB) hydrogels were shown to avoid capsule formation for 3 months after subcutaneous implantation in mice, which was the longest time a biomaterial had mitigated this response (*8*, *9*). However, the mechanical properties of those zwitterionic hydrogels were rather weak because of their super-hydrophilic characteristics. A simple solution to increase the mechanical properties of materials is to add a hydrophobic component, but which increases protein adsorption and induces fibrous capsule formation. In parallel, substantial progress has been made to strengthen the mechanical properties of various hydrogels, such as double-network, reversible cross-linking; molecular sliding; and more (*21*–*28*). While many hydrogels are shown to have low protein adsorption and cell adhesion, they are still far from long-term fibrous capsule resistance. Thus, our objective in this study is to develop a high-strength pure zwitterionic elastomer with excellent long-term fibrous capsule resistance.

Here, we present a zwitterionic-elastomeric-networked (ZEN) hydrogel (Fig. 1A), realized by integrating two weak zwitterionic hydrogels: pCB and poly(sulfobetaine) (pSB). In this pCB/pSB ZEN hydrogel, pCB is the minor component, forming a tightly cross-linked network to create elasticity, while pSB is the major component, forming a loosely cross-linked network to provide viscosity (*21*). Notably, the pCB network has a high swellability that could integrate a considerable amount of the pSB network, while the pSB network "locks" the entire hydrogel via strong inter- and intramolecular electrostatic interactions (*29*, *30*). The new mechanism of combining the excellent swellability and the "locking" effect allows us to achieve ZEN hydrogels with high mechanical strengths from only pure zwitterionic constituents. We have further demonstrated that three parameters (type, combination, and composition of zwitterionic constituents) are the key to achieve ZEN hydrogels. The pCB/pSB ZEN hydrogel was demonstrated to resist fibrous capsule formation after subcutaneous implantation in mice for up to 1 year.

RESULTS AND DISCUSSION

Mechanical properties and design principles of ZEN hydrogels

Conventional hydrogels for medical applications, such as poly(ethylene glycol) (PEG) and poly(2-hydroxyethyl methacrylate) (pHEMA), have relatively weak mechanical properties, with compressive fracture stresses ranging from 0.6 to 3 MPa (*21*, *22*, *31*). Traditional zwitterionic hydrogels, such as pCB, pSB, and poly(2-methacryloyloxyethyl phosphorylcholine) (pMPC), are quite weak as well, having a limit of around 3 MPa (*6*, *13*). In contrast, the pCB/pSB ZEN hydrogel was able to be smoothly compressed to a strain of 99% with a fracture stress of 22.3 MPa and maintained its original shape upon release (Fig. 1, B and C, and fig. S1). Similarly, the pCB/pSB ZEN hydrogel

[1]Department of Chemical Engineering, University of Washington, Seattle, WA 98185, USA. [2]School of Chemical Engineering and Technology, and Key Laboratory of Systems Bioengineering of Ministry of Education, Tianjin University, Tianjin 300350, China. [3]Meinig School of Biomedical Engineering, Cornell University, Ithaca, NY 14853, USA.
*These authors contributed equally to this work.
†Corresponding author. Email: sjiang@uw.edu, sj19@cornell.edu

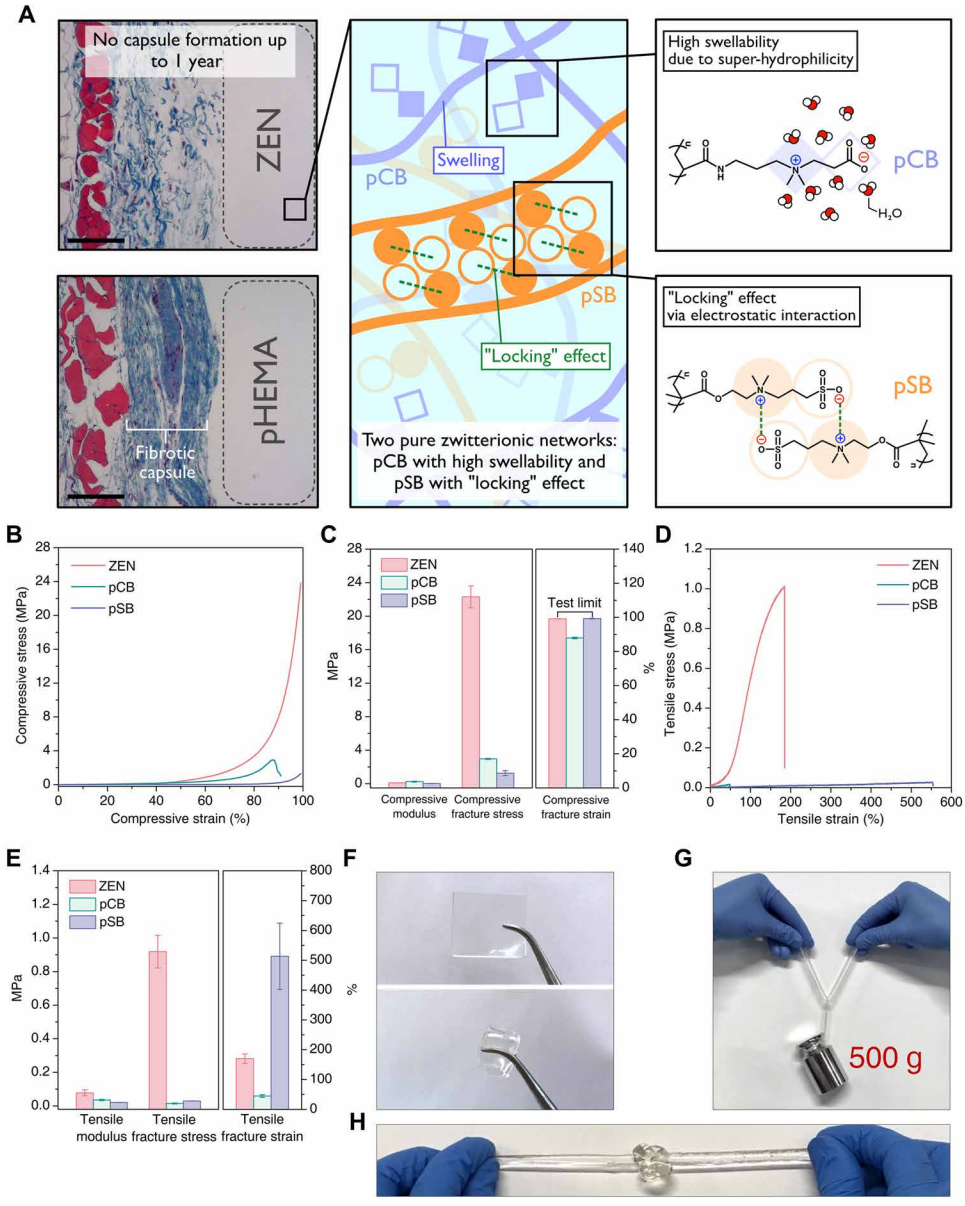

Fig. 1. pCB/pSB ZEN hydrogels with high mechanical properties. (**A**) Schematic illustration of the design principles of the high-strength poly(carboxybetaine) (pCB)/poly(sulfobetaine) (pSB) ZEN hydrogel. Left: Masson's trichrome staining results for skin tissues of mice with hydrogel subcutaneous implantation for 1 year. Skin tissue of mice that were implanted with poly(2-hydroxyethyl methacrylate) (pHEMA) hydrogel was set as positive control with fibrous capsule formation. Scale bars, 100 μm. (**B** to **E**) Representative uniaxial compressive curves (B); compressive modulus, fracture stress, and fracture strain (C); representative tensile curves (D); and tensile modulus, fracture stress, and fracture strain (E) of the pCB/pSB ZEN, pCB [1-4-0.1], and pSB [4-0.1-0.01] hydrogels. (**F**) The pCB/pSB ZEN hydrogel sheet can be stretched, twisted, and folded repeatedly without any visible damage observed. (**G** and **H**) The pCB/pSB ZEN hydrogel rope with a cross-sectional diameter of 6 mm can hold a weight of 500 g (G) and can tie knots without breaking (H). Note that *x*, *y*, and *z* for [*x*-*y*-*z*] represent the molar monomer concentration, cross-linker concentration [mole percent (mol %) with respect to the monomer], and initiator concentration (mol % with respect to the monomer), respectively. Photo credit: D. Dong (University of Washington, Tianjin University).

exhibited a large tensile strain of 169.9% with a fracture stress close to 1 MPa (Fig. 1, D and E), which is comparable to that of biological tissues such as blood vessels (*7*, *32*). The tensile curve of the pCB/pSB ZEN hydrogel behaved in an elastomeric manner without obvious stress yielding. Moreover, the pCB/pSB ZEN hydrogel could be fabricated into many shapes and was able to hold extensive deformation before returning to its original geometry (Fig. 1, F to H, and movies S1 and S2).

To elucidate the universal design principles of the ZEN hydrogels, we studied the structure-property relationship between the two zwitterionic networks: pCB and pSB. First, we carried out an orthogonal compressive test of a series of hydrogels consisting of three different pCB networks and seven pSB networks, each varying in monomer concentrations and cross-linker ratios (Fig. 2, A to C). The monomer, cross-linker, and initiator concentrations resulting in the optimal compressive fracture stress for the pCB/pSB hydrogel were 1-4-0.1 (monomer–cross-linker–initiator) for the pCB network and 4-0.1-0.01 for the pSB network. This indicated the importance of combining a higher cross-linked [4 mole percent (mol %)] pCB network to

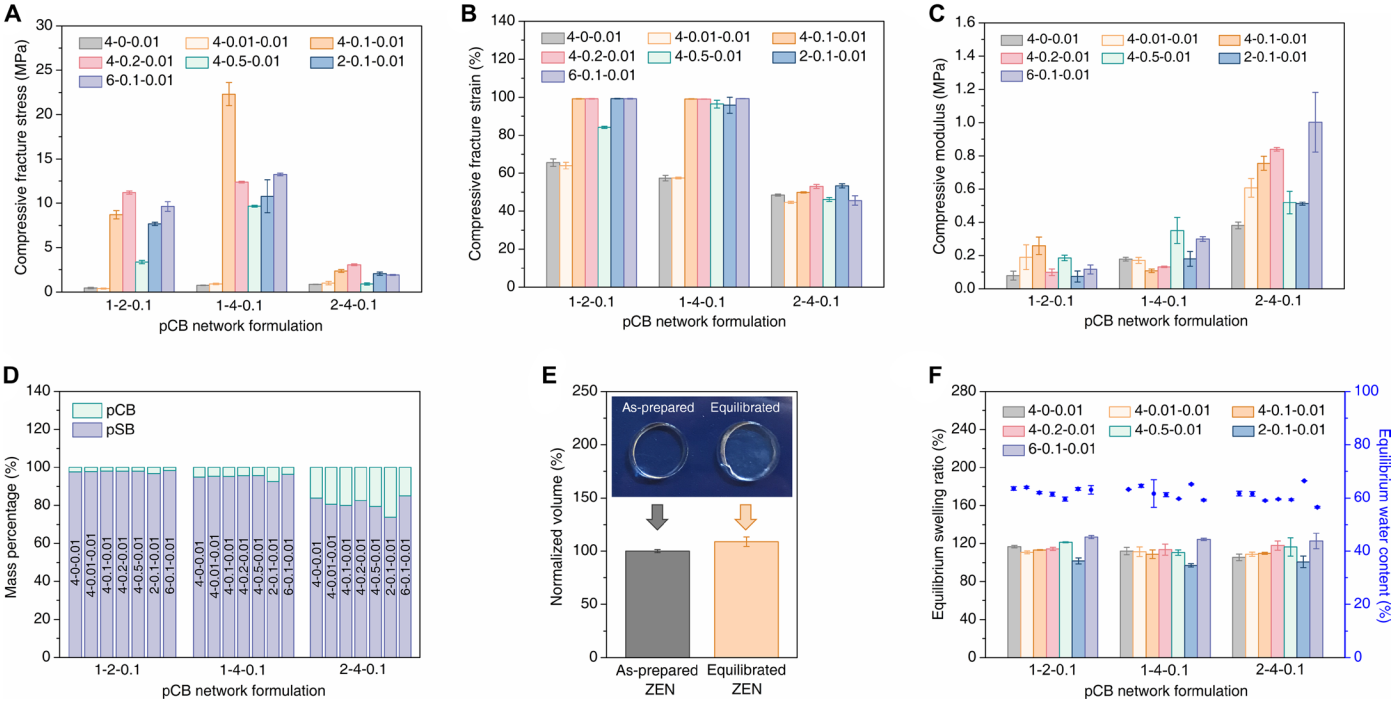

Fig. 2. Mechanical and swelling properties of a series of pCB/pSB hydrogels. (**A** to **D**) Compressive fracture stress (A), compressive fracture strain (B), compressive modulus (C), and component mass percentage (D) of a series of pCB/pSB hydrogels with combinations of three pCB network (1-2-0.1, 1-4-0.1, and 2-4-0.1) and seven pSB network (4-0-0.01, 4-0.01-0.01, 4-0.1-0.01, 4-0.2-0.01, 4-0.5-0.01, 2-0.1-0.01, and 6-0.1-0.01) component ratios. (**E**) Volume change of the pCB/pSB ZEN hydrogel before and after reaching equilibrium in water. The volume of the equilibrated pCB/pSB ZEN hydrogel was normalized to the corresponding as-prepared ZEN hydrogel. Photo credit: D. Dong (University of Washington, Tianjin University). (**F**) Equilibrium swelling ratios and equilibrium water contents of a series of pCB/pSB hydrogels with combinations of three pCB network and seven pSB network component ratios. Note that *x*, *y*, and *z* for *x*-*y*-*z* represent the molar monomer concentration, cross-linker concentration (mol % with respect to the monomer), and initiator concentration (mol % with respect to the monomer) of the corresponding network, respectively.

provide elasticity, with a lower cross-linking density (0.1 mol %) in the pSB network to provide viscosity. Cross-linking density of the pSB network lower than 0.1 mol % would contribute to a fragile pCB/pSB hydrogel regardless of the composition of the pCB network. The mass percentages of the pSB and pCB components corresponding to the optimal mechanical strength were 95 and 5%, respectively, which made pSB the major component and pCB the minor component (Fig. 2D). A considerable amount of the pSB component was able to be integrated because of the high swellability of the pCB component. Moreover, the critical locking effect was observed after the pCB/pSB ZEN hydrogel was immersed in water for swelling to equilibrium (Fig. 2E). The volume of the equilibrated pCB/pSB ZEN hydrogel increased only slightly (~9%) from its as-prepared state, while its parent pCB hydrogel (1-4-0.1, monomer–cross-linker–initiator) had a large volume increase of about 500%. Under the same orthogonal study (Fig. 2F), we observed other pCB/pSB formulations to also exhibit only small increases in volume, with equilibrium water contents (EWCs) kept around 60 to 66%. This suggested the locking effect to be universal in the pCB/pSB hydrogel system when pSB was the major component network.

The first series of structure-property experiments above showed that the high strength of the pCB/pSB ZEN hydrogel was derived from an optimal elasticity/viscosity ratio of the two networks, which was achieved through the two key concepts: the high swellability of the pCB minor component network and a locking effect generated by the pSB major component network. To demonstrate the importance of these two key concepts, we next compared other minor component/major component combinations of the two zwitterionic networks: pCB/pCB, pSB/pCB, and pSB/pSB. We first conducted an orthogonal compressive test for pCB/pCB hydrogels to examine the effect when pSB is not the major component network (Fig. 3, A, D, and E, and fig. S2). As expected, without pSB as the locking major component network, all pCB/pCB hydrogels exhibited a large volume increase after reaching equilibrium in water (Fig. 3F), resulting in weak mechanical properties. The highest fracture stress among all pCB/pCB combinations was only one-fifth that of the pCB/pSB ZEN hydrogel. In the pSB/pCB system (Fig. 3, B, D, E, and F) where pSB is the minor component network, there was also no locking effect, as the hydrogel increased 120% of its original size after reaching equilibration, resulting in a fracture stress of only around 1 MPa. On the other hand, in the pSB/pSB system (Fig. 3, C to F), the locking effect was observed as expected, along with a small increase in equilibrated volume of around 7.9%. Even though all the pSB/pSB hydrogels exhibited improved mechanical strength when compared to traditional pSB hydrogels—with the optimal pSB/pSB (1-4-0.1/4-0.1-0.01) formulation having a compressive fracture stress around 10 MPa—the maximum compressive fracture stress was only half of that of the pCB/pSB ZEN hydrogel. This could be due to the inferior swellability of pSB as the minor component network, resulting in a lower mass percentage of the major component network (less than 85%), which affected the mechanical strength of the pSB/pSB hydrogels. Together, these results confirm the essential design principles of the ZEN hydrogels: Having a minor component network with high swellability and a major component network with the locking

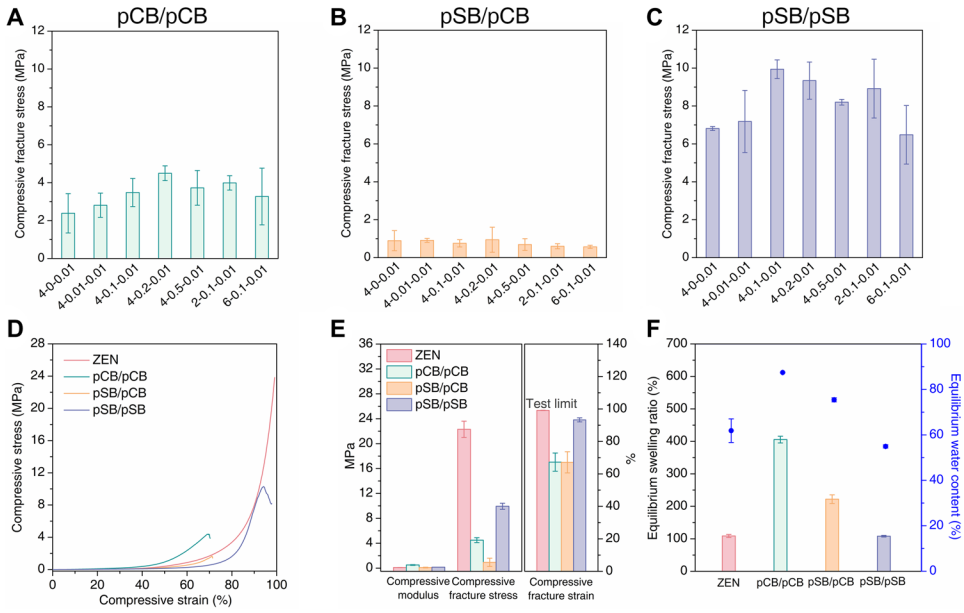

Fig. 3. Essential design principles of the ZEN hydrogels. A minor component network with high swellability and a major component network with the locking effect are the essential design principles of the ZEN hydrogels. (**A** to **C**) Compressive fracture stress of pCB/pCB (A), pSB/pCB (B), and pSB/pSB hydrogels (C). The minor component network of these hydrogels was made according to the composition of 1-4-0.1. The major component network was made according to seven different compositions as indicated on the *x* axis. *x*, *y*, and *z* for *x*-*y*-*z* represent the molar monomer concentration, cross-linker concentration (mol % with respect to the monomer), and initiator concentration (mol % with respect to the monomer) of the corresponding network, respectively. (**D** to **F**) Representative compressive curves (D); compressive modulus, fracture stress, and fracture strain (E); and equilibrium swelling ratios and equilibrium water contents (F) of the pCB/pSB ZEN, pCB/pCB, pSB/pCB, and pSB/pSB hydrogels. The pCB/pSB ZEN and pSB/pSB hydrogels were made according to the composition of 1-4-0.1/4-0.1-0.01, while pCB/pCB and pSB/pCB hydrogels were made according to the composition of 1-4-0.1/4-0.2-0.01. Note that *x*, *y*, and *z* for x_1-y_1-z_1/x_2-y_2-z_2 represent the molar monomer concentration, cross-linker concentration (mol % with respect to the monomer), and initiator concentration (mol % with respect to the monomer) for the two component networks, respectively.

effect is critical to realize ZEN hydrogels with an optimal elasticity/viscosity ratio. The ZEN hydrogels could also be achieved when other super-hydrophilic zwitterionic materials such as poly(trimethylamine *N*-oxide) (pTMAO) (*33*) with high swellability were used as the minor component network and pSB was used as the major component network with the locking effect, further resonating with the two key concepts of making the ZEN hydrogels (fig. S3).

Long-term subcutaneous implantation of ZEN hydrogels in mice

After elucidating the principles behind the high strength of the ZEN hydrogels, we continued to examine how living tissues respond to the presence of pCB/pSB ZEN hydrogels upon implantation. While many polymeric hydrogels, such as those based on PEG and pHEMA, have been developed for tissue engineering and regenerative medicine (*11*), they frequently elicit fibrous capsule formation upon subcutaneous implantation (*34*, *35*). This is the result of triggering the foreign body reaction, a physiological response toward synthetic materials initiated by nonspecific protein adsorption onto implant surfaces, followed by cell adhesion and the subsequent formation of fibrous tissue around the implants (*6*, *8*–*10*). This "capsule" acts as an impermeable barrier that impedes nutrient and signal transport, often culminating in implant failure (*11*). As nonspecific protein adsorption and cell adhesion are the initial steps in this response, we first challenged the pCB/pSB ZEN hydrogel with in vitro exposure to fibrinogen, undiluted human serum, rat-derived platelet-rich plasma (PRP), and two adherent cell lines [rat pancreatic β cells (RIN-m5F) and murine DC 2.4 dendritic cells]. The results were compared to those of pCB, pSB, and pHEMA hydrogels (figs. S4 and S5). We found the pCB/pSB ZEN hydrogel to maintain excellent non-fouling properties (**$P < 0.01$) similar to its parent zwitterionic hydrogels, pCB and pSB, but the pHEMA hydrogel was unable to prevent nonspecific protein adsorption and cell adhesion as effectively ($^{\#\#}P < 0.01$). The pCB/pSB ZEN hydrogel also exhibited excellent stability after sterilization—even after three rounds of routine autoclaving cycles (121°C, 30 min each), the pCB/pSB ZEN hydrogel retained its non-fouling properties against proteins, platelets, and cells (**$P < 0.01$) (fig. S6).

Encouraged by the unique combination of strength, durability, and non-fouling properties exhibited by the pCB/pSB ZEN hydrogel, we last explored its long-term in vivo fibrous capsule resistance upon implantation. Both pCB/pSB ZEN and pHEMA hydrogel samples were subcutaneously implanted on the back of immunocompetent C57BL/6 mice for up to 1 year. Skin tissues in contact with the hydrogel samples were collected from mice at various time intervals (1, 4, and 12 weeks and 1 year) to evaluate potential fibrous capsule formation. Positive controls were skin tissues collected from mice that were implanted with pHEMA hydrogels (*8*), while negative controls were collected from mice that did not undergo any surgeries or other experiments. All skin tissues were further treated with hematoxylin and eosin (H&E) and Masson's trichrome staining for histological analysis. One week after implantation, basophilic discoloration and obvious cell accumulation were observed at the tissue interface in direct contact with pHEMA hydrogels, indicating an acute inflammatory response (Fig. 4A). As inflammation is known to trigger recruitment of collagen-secreting fibroblasts to encapsulate

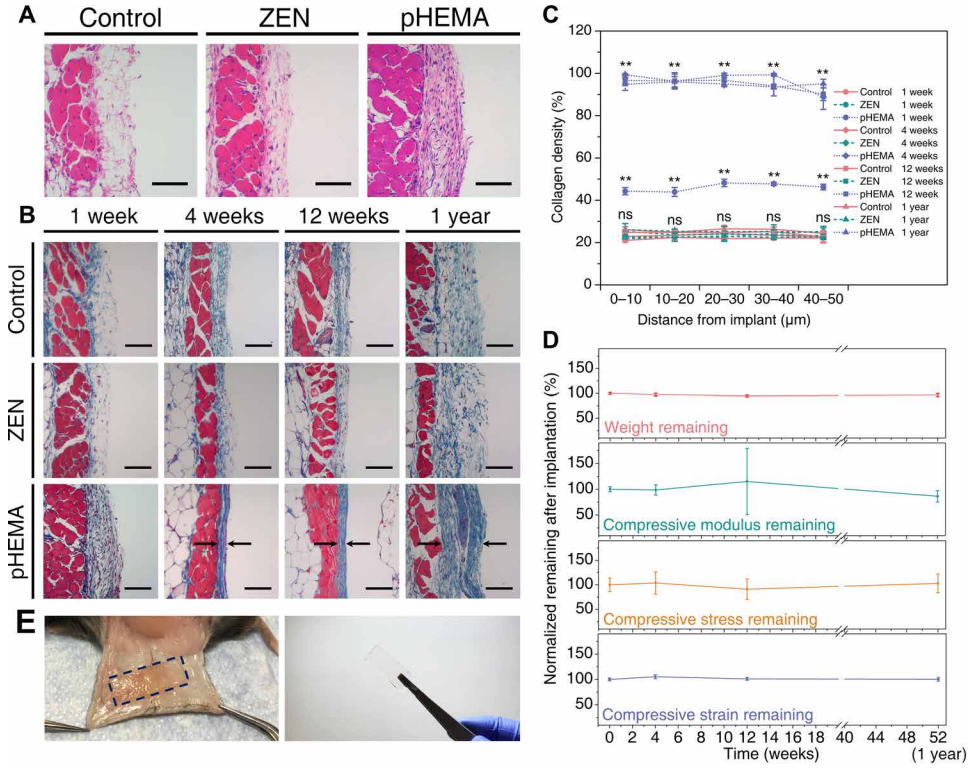

Fig. 4. pCB/pSB ZEN hydrogels present long-term fibrous capsule resistance and durability after subcutaneous implantation in mice up to 1 year. (**A** and **B**) H&E staining for skin tissues in contact with the ZEN and pHEMA hydrogels after 1 week of implantation (A). The basophilic discoloration and increased cell counts (stained dark purple) at the interface in contact with pHEMA hydrogels indicate the accumulation of cells into the interface. Masson's trichrome staining for skin tissues with different hydrogel samples after implantation for 1, 4, and 12 weeks, and 1 year (B). Black arrows indicate the fibrous capsule. Positive controls were skin tissues collected from mice that were implanted with pHEMA hydrogels, while negative controls were collected from mice that did not undergo any surgeries or other experiments. Scale bars, 100 μm. $n = 3$ for all the implantation experiments (three mice per experiment group/condition and two hydrogel samples per mouse for ZEN or pHEMA hydrogels implantation). (**C**) Collagen density in the skin tissues adjacent to the hydrogel samples after implantation for 1, 4, and 12 weeks, and 1 year. Data were collected in the skin tissues within 50 μm from the interface (at 10-μm increments). $^{**}P < 0.01$ versus control; ns, no statistical difference versus control. (**D**) Normalized dry weight and compressive strength (compressive modulus, stress, and strain) remaining of the ZEN hydrogels during the implantation for 1 year. All data were normalized to that of the original ZEN hydrogels before implantation (0 weeks). (**E**) Representative images of the implanted mice and retrieved ZEN hydrogels after 1-year implantation. Photo credit: C. Tsao (University of Washington).

and isolate the foreign material (*10*, *11*), it was expected to observe the formation of an initial collagen layer in these mice after 1 week (Fig. 4, B and C, $^{**}P < 0.01$). By the fourth week of pHEMA hydrogel implantation, a dense and mature collagenous capsule had formed, which further thickened after 1 year (Fig. 4, B and C).

In contrast, few to no cells were observed at the interface between tissue and implanted pCB/pSB ZEN hydrogels after 1 week (Fig. 4A), similar to that of the negative controls, suggesting that they elicited little or no acute inflammation—a phenomenon derived from excellent non-fouling properties (*8*, *9*, *13*). Over the entire span of this study, skin tissues adjacent to pCB/pSB ZEN hydrogels showed neither signs of inflammation (fig. S7) nor any dense fibrous capsule formation, but instead a loose subcutaneous structure similar to that of the negative control skin tissues (Fig. 4, B and C). Furthermore, the pCB/pSB ZEN hydrogel samples maintained their shape and were highly durable, with no obvious degradation and loss in mechanical properties after one full year of implantation (Fig. 4, D and E). This suggests that ZEN hydrogel materials are able to maintain long-term fibrous capsule resistance and durability in vivo.

In summary, we report here a "ZEN" hydrogel exhibiting a unique combination of mechanical strength and long-term fibrous capsule resistance. The key feature of a ZEN hydrogel is its composition from two different pure zwitterionic networks—a tightly cross-linked minor component network that has high swellability and a loosely cross-linked major component network that exhibits critical locking effect. We found the pCB/pSB ZEN hydrogel to exhibit excellent elasticity under extensive deformation, mitigate the fibrous capsule formation, and remain stable without degradation or loss of mechanical strength when implanted subcutaneously for up to 1 year in mice. We envision the durability and fibrous capsule resistance of ZEN hydrogels to provide a new route to long-standing ambitions of implantable materials, such as cartilage replacement, tissue repair, and catheters.

MATERIALS AND METHODS

Materials

[2-(Methacryloyloxy)ethyl]dimethyl-(3-sulfopropyl)ammonium hydroxide (SB; 95%) and 2-hydroxyethyl methacrylate (HEMA; 97%)

were obtained from Sigma-Aldrich (Milwaukee, WI), and purification was carried out to remove inhibitor before use. 3-[3-(Acrylamidopropyl) dimethylammonio]propionate (CB) and trimethylamine *N*-oxide (TMAO) monomer were synthesized following our previous reports (*33*, *36*). *N*,*N*′-Methylenebisacrylamide (MBAA; ≥98%), 2-hydroxy-2-methylpropiophenone (photoinitiator 1173, 97%), ammonium persulfate (≥98%), *N*,*N*,*N*′,*N*′-tetramethylethylenediamine (TEMED; 99%), fibrinogen from human plasma (≥80% clottable protein), *o*-phenylenediamine (OPD; ≥98%), and phosphate-buffered saline [PBS; 10 mM phosphate, 138 mM sodium chloride, and 2.7 mM potassium chloride (pH 7.4)] were purchased from Sigma-Aldrich (Milwaukee, WI). Horseradish peroxidase (HRP)–conjugated anti-fibrinogen was purchased from Alpha Diagnostic International (San Antonio, TX). Human serum with citrate phosphate dextrose (CPD), pooled and mixed gender, was purchased from BioChemed Services (Winchester, VA). Pierce LDH Cytotoxicity Assay Kit and Pierce BCA Protein Assay Kit were purchased from Thermo Fisher Scientific (Bothell, WA). Rat pancreas/islet of Langerhans RIN-m5F cell line was purchased from the American Type Culture Collection (ATCC) (Manassas, VA), and mouse dendritic cell line DC 2.4 was a gift from K. L. Rock (University of Massachusetts Medical Center, Worcester, MA).

Preparation of hydrogels

All the poly(CB)/poly(SB) (pCB/pSB) hydrogels were prepared following a two-step sequential free-radical polymerization method. In general, take the synthesis of pCB/pSB ZEN hydrogel for example, the ZEN hydrogel consists of the formation of the pCB minor component network followed by the construction of the pSB major component network. In the first step, the zwitterionic minor component network (ZMN1) pCB hydrogel was synthesized by photopolymerization using 1 m (molality) of CB monomer, 4 mol % of cross-linker, and 0.1 mol % of photoinitiator 1173 (molar percentages both were relative to the CB monomer) in the transparent sheet mold or the tubular rod mold under ultraviolet (UV) irradiation with a wavelength of 302 nm and a power of 6 W for 6 hours under a nitrogen atmosphere. In the second step, the prepared pCB ZMN1 hydrogels were immersed into the precursor solution of the zwitterionic major component network (ZMN2) containing 4 m of SB monomer, 0.1 mol % of MBAA cross-linker, and 0.01 mol % of photoinitiator 1173 (molar percentages were both relative to the SB monomer) overnight. The fully swollen ZMN1 hydrogels containing the precursor for ZMN2 were further polymerized by UV irradiation with a wavelength of 302 nm and 6-W power for 6 hours under a nitrogen atmosphere. After this two-step synthesis, the as-prepared pCB/pSB ZEN hydrogel was immersed in water for at least 1 day with at least three water replacements until it reached the swelling equilibrium. All other different two–zwitterionic network hydrogels were prepared following the same method but with different zwitterionic components and composition ratios. Hereafter, the two–zwitterionic network hydrogels were named pA/pB [x_1-y_1-z_1/x_2-y_2-z_2], where A and B were the abbreviations of the zwitterionic monomer used to form ZMN1 and ZMN2, respectively; x_i, y_i, and z_i (i = 1 and 2) were monomer molality (m) and cross-linker and initiator concentration (mol % with respect to the corresponding monomer) of ZMNi, respectively.

For parent zwitterionic hydrogel preparation, the pCB hydrogel was prepared following the same protocol of pCB ZMN1 hydrogel as above. The pSB hydrogel was synthesized by photopolymerization using 4 m of SB monomer, 0.1 mol % of MBAA cross-linker, and 0.01 mol % of photoinitiator 1173 (molar percentages were both relative to the SB monomer) in a transparent sheet mold under UV irradiation with a wavelength of 302 nm and 6-W power for 6 hours under a nitrogen atmosphere. The parent hydrogels were respectively named pCB [1-4-0.1] and pSB [4-0.1-0.01] similar to described above, where x, y, and z for [x-y-z] represent the molar monomer concentration (molality, m) and cross-linker concentration (mol % with respect to the monomer) and initiator concentration (mol % with respect to the monomer), respectively. For the pHEMA hydrogel, 1 m of HEMA monomer, 4 mol % of MBAA cross-linker, 0.1 mol % of initiator ammonium persulfate, and 0.1 mol % of accelerator TEMED (molar percentages were both relative to the HEMA monomer) were mixed in ethanol/water (1:1, v/v) solution and then injected into the sheet mold to polymerize at 37°C for 24 hours. The as-prepared pHEMA hydrogel was then allowed to swell in deionized water for at least 2 days with water replacements until all the ethanol was removed and the hydrogel turned transparent. All other as-prepared hydrogels were also equilibrated in deionized water or PBS before use.

ESR and EWC test

The equilibrium swelling ratios (ESRs) of equilibrated hydrogels to their as-prepared state were evaluated via a dimension measurement method. The diameters (r_1) and heights (h_1) of as-prepared two–zwitterionic network hydrogels fabricated from ZMN1 disks with fixed dimensions of Φ5 mm by 0.5 mm were measured. The as-prepared hydrogels were then soaked in deionized water for 2 days for complete swelling, and the diameters (r_2) and heights (h_2) of their corresponding equilibrated state were measured. The ESRs were calculated as follows

$$\mathrm{ESR} = \frac{r_2^2 \times h_2}{r_1^2 \times h_1} \times 100\% \quad (1)$$

The EWCs of equilibrated hydrogels were measured through a gravimetric method. Hydrogel disks (10 mm in diameter and 1 mm in thickness) were allowed to swell in deionized water until reaching equilibrium at 37°C. The equilibrated samples were taken out, and their wet masses (M_w) were measured after the removal of excess water on the surface by rolling them on the filter paper. The samples were then snap-frozen in liquid nitrogen and lyophilized for 2 days until complete dryness is achieved and their dry masses (M_d) were measured. The EWCs were calculated as follows

$$\mathrm{EWC} = \frac{M_w - M_d}{M_w} \times 100\% \quad (2)$$

Each measurement was performed in triplicate (independent replicates).

Compressive and tensile test

Hydrogels were allowed to reach swelling equilibrium in deionized water for 1 day at room temperature before testing. The compressive property of hydrogels was tested on a universal testing machine (Instron 5543A, Instron Corp., Norwood, MA) with a 10-kN load cell at room temperature. Biopsy punch was used to punch equilibrated hydrogels into 5-mm-diameter and 2-mm-thick cylinders. The crosshead speed was set at 1 mm/min, and the test limit of compressive strain was set at 99% to protect the machine. The tensile property of hydrogels was tested on a universal testing machine

(WDW-05, Si Pai Inc., China) with a 500-N load cell at room temperature. The equilibrium sheet samples were cut into dumbbell shape with a length of 30 mm, a gauge length of 12 mm, a width of 2 mm, and a thickness of 1 mm, and the crosshead speed was set at 50 mm/min. Each measurement was performed at least in triplicate (independent replicates).

Fibrinogen adhesion test by enzyme-linked immunosorbent assay

Human fibrinogen adhesion test of hydrogels was performed in 24-well tissue culture polystyrene (TCPS) plates using an enzyme-linked immunosorbent assay method following our previous reports (*7*, *37*). Before the experiment, all the tested hydrogels were equilibrated in PBS and then cut into uniform disks (5 mm in diameter and 1 mm in thickness) with the biopsy punch. Each sample disk was first incubated in 1 ml of fibrinogen solution (1 mg/ml; freshly prepared in PBS) at 37°C for 1.5 hours. Before being transferred into new wells, the samples were rinsed with 5 × 2 ml of PBS to remove dissociative fibrinogen. One milliliter of HRP-conjugated anti-fibrinogen solution (1 μg/ml, in PBS) was then added in each well, followed by incubation at room temperature for 1.5 hours. All the samples were then transferred to new wells after another five washes with PBS. One milliliter of OPD solution [1 mg/ml, with 0.1 M citrate phosphate (pH 5.0)] containing 0.03% hydrogen peroxide was added. After 15 min of incubation at room temperature, the enzymatic reaction was stopped by adding 1 ml of 1 N HCl. The absorbance values at 492 nm of all the samples were recorded by a plate reader (Cytation 3, BioTek, Winooski, VT) and were normalized to that of TCPS (96-well, control). Each measurement was performed in quadruplicate (independent replicates).

Serum fouling test by BCA assay

Human serum fouling of the hydrogels was evaluated via the bicinchoninic acid (BCA) method. Pre-equilibrated hydrogel disks in PBS (5 mm in diameter and 1 mm in thickness) were suspended into 400 μl of undiluted human pooled serum in 24-well TCPS plates with one disk per well followed by incubation at 37°C for 2 hours. Before being transferred into new wells, all the samples were rinsed five times with 1 ml of PBS to remove the dissociative proteins. A BCA assay was then directly carried out to determine the amount of proteins adsorbed on the hydrogel, and the absorbance values at 562 nm of all the samples were recorded by a plate reader and were normalized to that of TCPS (96-well, control). Each measurement was performed in triplicate (independent replicates).

Platelet adhesion analysis by LDH assay

Platelets used for adhesion analysis were freshly collected from the blood of two 11- to 13-week-old female Sprague-Dawley rats. Fresh blood collected in a Becton Dickinson (Franklin Lakes, NJ) plasma tube [75 United States Pharmacopeia (USP) units of sodium heparin (spray-coated)] was then immediately centrifuged at 200*g* for 10 min to get PRP. The residue was further centrifuged at 2000*g* for 20 min to obtain platelet-poor plasma (PPP). PRP and PPP were gently remixed, and the final platelet density was adjusted to 2×10^8 ml^{-1}. Pre-equilibrated hydrogel disks in PBS (5 mm in diameter and 1 mm in thickness) were placed in 24-well TCPS plates with one disk per well, immersed with 400 μl of final platelet solution, and incubated at 37°C for 3 hours. After incubation, the disks were rinsed five times with 1 ml of PBS and then transferred into new wells. The number of adhered platelets was determined by the lactate dehydrogenase (LDH) assay. For LDH assay, the rinsed samples were soaked in 24-well TCPS plates with one disk per well, 300 μl of PBS, and 10 μl of 10× lysis buffer and incubated at 37°C, 5% CO_2 for 45 min. Fifty-microliter reaction mixtures were then added into each well and incubated at room temperature for 30 min in the dark. To stop the reaction, 50 μl of STOP solution was added to each well and mixed by gentle pipetting. Last, 200 μl of the mixture was taken out from each well, and the absorbance at 490 and 680 nm was measured by a platelet reader. The LDH activity was determined by subtracting the absorbance value of 680 nm from that of 490 nm. Data were normalized to that of TCPS (96-well, control). Each measurement was performed in triplicate (independent replicates).

Cell adhesion assay

Rat pancreatic β cells (RIN-m5F) and murine DC 2.4 dendritic cells were selected for the cell adhesion assay of the hydrogels. In brief, PBS pre-equilibrated and UV-sterilized hydrogels disks (5 mm in diameter and 1 mm in thickness) were placed individually into the wells of a 96-well plate. RIN-m5F [suspended in ATCC-formulated RPMI 1640 with 10% fetal bovine serum (FBS)] or DC 2.4 cells (suspended in RPMI 1640 with 10% FBS, 1× L-glutamine, 1× nonessential amino acids, 1× HEPES buffer solution, and 0.0054× β-mercaptoethanol) were seeded onto the hydrogels at a density of 1×10^5 or 5×10^4 cells/ml, respectively, and allowed to grow for 24 hours at 37°C in a humidified atmosphere with 5% CO_2. The medium was then removed, and the hydrogels were gently washed with PBS and reimmersed with PBS. For optical imaging, cell adhesion and cellular morphology on the samples were observed at ×200 magnification using a microscope (Nikon Eclipse 80i). For quantitative analysis of adhered cells, the samples were gently transferred to new wells, and then the LDH assay was carried out following the protocol as described above. All the data were normalized to that of TCPS (96-well, control). Each measurement was performed in triplicate (independent replicates).

Hydrogel sterilization by autoclaving

The pCB/pSB ZEN hydrogels were sterilized via a standard autoclaving method. As-prepared ZEN hydrogels were soaked in water or PBS until equilibrium and then sterilized at 121°C for 30 min together with corresponding soaking solutions. The sterilized hydrogels were then cooled to room temperature for further use or test. Hydrogels that experienced one to three rounds of such heating-cooling autoclaving sterilization process were named ZEN-R1, ZEN-R2, and ZEN-R3, respectively. The subsequent protein and cell adhesion tests of autoclaved ZEN hydrogels all followed the protocols described as above.

In vivo implantation of ZEN hydrogels

Six- to 8-week-old male C57BL/6 mice were purchased from Charles River Laboratories. All the animal experiments were operated according to the federal guidelines and were approved by the University of Washington Institutional Animal Care and Use Committee. Subcutaneous implantation experiments were carried out to evaluate the foreign body reaction and fibrous capsule formation of pCB/pSB ZEN hydrogels. pHEMA hydrogel implantation was selected as positive controls according to our previous study (*8*). Negative controls were set by skin tissues of mice that did not undergo any surgeries or other experiments. ZEN hydrogel (with dimensions of 1 cm by 1 cm and 1 cm by 3 cm) and pHEMA hydrogel (with dimensions

of 1 cm by 1 cm) sheets were sterilized by autoclaving (121°C for 30 min in PBS) and UV (for 30 min), respectively, before implantation to prevent bacterial infection. The animal surgery was performed under anesthesia and aseptic conditions. In brief, each mouse was subcutaneously implanted with two ZEN or two pHEMA hydrogels symmetrically on the back, with one hydrogel on each side. The two hydrogel samples in all mice did not overlap throughout the whole study. Mice were anesthetized using 3% isoflurane and shaved. The area where the incision would be made was sterilized using iodine and 70% ethanol. A longitudinal incision (no longer than 2 cm) was made on the central dorsal surface using surgical scissors to provide access to the subcutaneous space. Subcutaneous pockets on either side of the incision were created with blunt forceps for the implantation of the hydrogel samples. After implantation, the incisions were closed using wound nylon sutures. Mice were monitored until recovery from anesthesia and housed for 1 week, 4 weeks, 12 weeks, or 1 year before retrieving samples. For each experiment group/condition, three different mice were implanted with hydrogel samples or not (as negative control) to provide statistical significance in the histological studies ($n = 3$). The researchers did not subjectively select starting materials or animals. No animals were lost before reaching their assigned end points.

Hydrogel retrieval and histological analysis

One week, 4 weeks, 12 weeks, or 1 year after implantation, mice were euthanized by CO_2 asphyxiation. The hydrogel samples together with the adjacent skin tissue were excised by cutting along the edge of the hydrogels. Negative controls were set by skin tissues of mice that did not undergo any surgeries or other experiments. The retrieved skin samples were then fixed in 4% paraformaldehyde for at least 2 days and then embedded in paraffin. Each retrieved skin tissue was sectioned with a thickness of 4 μm and mounted onto slides for histological staining. The inflammatory response was examined by staining with H&E, in which cell nuclei would appear dark purple and cell cytoplasm would appear pink. The fibrous capsule formation was stained using Masson's trichrome staining, which stains collagen blue, cell cytoplasm red, and cell nuclei black. Each stained slide was examined at ×100 magnification using a Leica DMIL Inverted Phase Contrast Microscope, and images were captured from at least three different sites alongside the interface between the subcutaneous skin tissue and the hydrogel. Examination and quantification of histological sections were done by three independent researches with at least three random images/fields per sample and per animal. Researchers were blinded to sample identity. The collagen densities of the subcutaneous skin tissues from different mice were analyzed with corresponding Masson's trichrome staining histological images (as described above) via the ImageJ software. In this study, the area proportion of the collagen (stained with blue) was defined as the collagen density of the selected area. For each image, the collagen densities were continuously collected in the subcutaneous skin tissue within 50 μm at 10-μm increments starting from the interface with the hydrogel sample (for negative control, starting from the internal surface adjacent to the back of the mouse). Each calculating area was rectangular (with dimensions of 10 μm by 100 μm) and was parallel to the interface. The starting calculating area was randomly selected alongside the interface for each image. Each skin tissue sample was analyzed in triplicate from three different corresponding histological images. For testing the dry weight and compressive strength of retrieved ZEN hydrogels, hydrogels were first slightly washed by deionized water after retrieval. Biopsy punch was then used to punch hydrogels into 5-mm-diameter disks. Compressive testing followed the same procedure as described above. Dry weights were measured after lyophilization. Each measurement was carried out in triplicate.

Statistical analysis

All data are expressed and presented as means and SD. Statistical analyses were performed with OriginPro 8.5 software. A two-tailed Student's t test was used for all statistical analyses. $P < 0.01$ was considered statistically significant.

SUPPLEMENTARY MATERIALS

Supplementary material for this article is available at http://advances.sciencemag.org/cgi/content/full/7/1/eabc5442/DC1

REFERENCES AND NOTES

1. K. Y. Lee, D. J. Mooney, Hydrogels for tissue engineering. *Chem. Rev.* **101**, 1869–1879 (2001).
2. R. Langer, D. A. Tirrell, Designing materials for biology and medicine. *Nature* **428**, 487–492 (2004).
3. D. Seliktar, Designing cell-compatible hydrogels for biomedical applications. *Science* **336**, 1124–1128 (2012).
4. T. Billiet, M. Vandenhaute, J. Schelfhout, S. Van Vlierberghe, P. Dubruel, A review of trends and limitations in hydrogel-rapid prototyping for tissue engineering. *Biomaterials* **33**, 6020–6041 (2012).
5. J. J. Green, J. H. Elisseeff, Mimicking biological functionality with polymers for biomedical applications. *Nature* **540**, 386–394 (2016).
6. A. L. Lewis, Phosphorylcholine-based polymers and their use in the prevention of biofouling. *Colloids Surf. B Biointerfaces* **18**, 261–275 (2000).
7. H.-C. Hung, P. Jain, P. Zhang, F. Sun, A. Sinclair, T. Bai, B. Li, K. Wu, C. Tsao, E. J. Liu, H. S. Sundaram, X. Lin, P. Farahani, T. Fujihara, S. Jiang, A coating-free nonfouling polymeric elastomer. *Adv. Mater.* **29**, 1700617 (2017).
8. L. Zhang, Z. Cao, T. Bai, L. Carr, J.-R. Ella-Menye, C. Irvin, B. D. Ratner, S. Jiang, Zwitterionic hydrogels implanted in mice resist the foreign-body reaction. *Nat. Biotechnol.* **31**, 553–556 (2013).
9. A. Azvolinsky, C. Schmidt, E. Waltz, S. Webb, 20 years of *Nature Biotechnology* biomedical research. *Nat. Biotechnol.* **34**, 262–266 (2016).
10. J. M. Anderson, A. Rodriguez, D. T. Chang, Foreign body reaction to biomaterials. *Semin. Immunol.* **20**, 86–100 (2008).
11. B. D. Ratner, Reducing capsular thickness and enhancing angiogenesis around implant drug release systems. *J. Control. Release* **78**, 211–218 (2002).
12. A. J. Vegas, O. Veiseh, J. C. Doloff, M. Ma, H. H. Tam, K. Bratlie, J. Li, A. R. Bader, E. Langan, K. Olejnik, P. Fenton, J. W. Kang, J. Hollister-Locke, M. A. Bochenek, A. Chiu, S. Siebert, K. Tang, S. Jhunjhunwala, S. Aresta-Dasilva, N. Dholakia, R. Thakrar, T. Vietti, M. Chen, J. Cohen, K. Siniakowicz, M. Qi, J. McGarrigle, S. Lyle, D. M. Harlan, D. L. Greiner, J. Oberholzer, G. C. Weir, R. Langer, D. G. Anderson, Combinatorial hydrogel library enables identification of materials that mitigate the foreign body response in primates. *Nat. Biotechnol.* **34**, 345–352 (2016).
13. S. Jiang, Z. Cao, Ultralow-fouling, functionalizable, and hydrolyzable zwitterionic materials and their derivatives for biological applications. *Adv. Mater.* **22**, 920–932 (2010).
14. K. Ishihara, T. Ueda, N. Nakabayashi, Preparation of phospholipid polymers and their properties as polymer hydrogel membranes. *Polym. J.* **22**, 355–360 (1990).
15. T. Bai, J. Li, A. Sinclair, S. Imren, F. Merriam, F. Sun, M. B. O'Kelly, C. Nourigat, P. Jain, J. J. Delrow, R. S. Basom, H.-C. Hung, P. Zhang, B. Li, S. Heimfeld, S. Jiang, C. Delaney, Expansion of primitive human hematopoietic stem cells by culture in a zwitterionic hydrogel. *Nat. Med.* **25**, 1566–1575 (2019).
16. A. J. Keefe, S. Jiang, Poly(zwitterionic)protein conjugates offer increased stability without sacrificing binding affinity or bioactivity. *Nat. Chem.* **4**, 59–63 (2012).
17. A. B. Lowe, C. L. McCormick, Synthesis and solution properties of zwitterionic polymers. *Chem. Rev.* **102**, 4177–4190 (2002).
18. P. Zhang, F. Sun, C. Tsao, S. Liu, P. Jain, A. Sinclair, H.-C. Hung, T. Bai, K. Wu, S. Jiang, Zwitterionic gel encapsulation promotes protein stability, enhances pharmacokinetics, and reduces immunogenicity. *Proc. Natl. Acad. Sci. U.S.A.* **112**, 12046–12051 (2015).
19. T. Moro, Y. Takatori, K. Ishihara, T. Konno, Y. Takigawa, T. Matsushita, U.-i. Chung, K. Nakamura, H. Kawaguchi, Surface grafting of artificial joints with a biocompatible polymer for preventing periprosthetic osteolysis. *Nat. Mater.* **3**, 829–836 (2004).
20. J. B. Schlenoff, Zwitteration: Coating surfaces with zwitterionic functionality to reduce nonspecific adsorption. *Langmuir* **30**, 9625–9636 (2014).

21. J. P. Gong, Y. Katsuyama, T. Kurokawa, Y. Osada, Double-network hydrogels with extremely high mechanical strength. *Adv. Mater.* **15**, 1155–1158 (2003).
22. J.-Y. Sun, X. Zhao, W. R. K. Illeperuma, O. Chaudhuri, K. H. Oh, D. J. Mooney, J. J. Vlassak, Z. Suo, Highly stretchable and tough hydrogels. *Nature* **489**, 133–136 (2012).
23. T. L. Sun, T. Kurokawa, S. Kuroda, A. Bin Ihsan, T. Akasaki, K. Sato, M. A. Haque, T. Nakajima, J. P. Gong, Physical hydrogels composed of polyampholytes demonstrate high toughness and viscoelasticity. *Nat. Mater.* **12**, 932–937 (2013).
24. H. Kamata, Y. Akagi, Y. Kayasuga-Kariya, U.-i. Chung, T. Sakai, "Nonswellable" hydrogel without mechanical hysteresis. *Science* **343**, 873–875 (2014).
25. X. Zhao, Multi-scale multi-mechanism design of tough hydrogels: Building dissipation into stretchy networks. *Soft Matter* **10**, 672–687 (2014).
26. H. Yuk, T. Zhang, G. A. Parada, X. Liu, X. Zhao, Skin-inspired hydrogel–elastomer hybrids with robust interfaces and functional microstructures. *Nat. Commun.* **7**, 12028 (2016).
27. Y. S. Zhang, A. Khademhosseini, Advances in engineering hydrogels. *Science* **356**, eaaf3627 (2017).
28. T. Matsuda, R. Kawakami, R. Namba, T. Nakajima, J. P. Gong, Mechanoresponsive self-growing hydrogels inspired by muscle training. *Science* **363**, 504–508 (2019).
29. Q. Shao, L. Mi, X. Han, T. Bai, S. Liu, Y. Li, S. Jiang, Differences in cationic and anionic charge densities dictate zwitterionic associations and stimuli responses. *J. Phys. Chem. B* **118**, 6956–6962 (2014).
30. Q. Shao, S. Jiang, Molecular understanding and design of zwitterionic materials. *Adv. Mater.* **27**, 15–26 (2015).
31. S. Lin-Gibson, R. L. Jones, N. R. Washburn, F. Horkay, Structure–property relationships of photopolymerizable poly(ethylene glycol) dimethacrylate hydrogels. *Macromolecules* **38**, 2897–2902 (2005).
32. G. Konig, T. N. McAllister, N. Dusserre, S. A. Garrido, C. Iyican, A. Marini, A. Fiorillo, H. Avila, W. Wystrychowski, K. Zagalski, M. Maruszewski, A. L. Jones, L. Cierpka, L. M. de la Fuente, N. L'Heureux, Mechanical properties of completely autologous human tissue engineered blood vessels compared to human saphenous vein and mammary artery. *Biomaterials* **30**, 1542–1550 (2009).
33. B. Li, P. Jain, J. Ma, J. K. Smith, Z. Yuan, H.-C. Hung, Y. He, X. Lin, K. Wu, J. Pfaendtner, S. Jiang, Trimethylamine *N*-oxide–derived zwitterionic polymers: A new class of ultralow fouling bioinspired materials. *Sci. Adv.* **5**, eaaw9562 (2019).
34. M. D. Swartzlander, C. A. Barnes, A. K. Blakney, J. L. Kaar, T. R. Kyriakides, S. J. Bryant, Linking the foreign body response and protein adsorption to PEG-based hydrogels using proteomics. *Biomaterials* **41**, 26–36 (2015).
35. P. Fleckman, M. Usui, G. Zhao, R. Underwood, M. Maginness, A. Marshall, C. Glaister, B. Ratner, J. Olerud, Cutaneous and inflammatory response to long-term percutaneous implants of sphere-templated porous/solid poly(HEMA) and silicone in mice. *J. Biomed. Mater. Res. A* **100**, 1256–1268 (2012).
36. Z. Zhang, H. Vaisocherová, G. Cheng, W. Yang, H. Xue, S. Jiang, Nonfouling behavior of polycarboxybetaine-grafted surfaces: Structural and environmental effects. *Biomacromolecules* **9**, 2686–2692 (2008).
37. S. Chen, S. Jiang, An new avenue to nonfouling materials. *Adv. Mater.* **20**, 335–338 (2008).

Acknowledgments: We thank the Histology and Imaging Core (HIC) at the University of Washington for performing H&E and Masson's trichrome staining. **Funding:** We acknowledge the Office of Naval Research (N00014-16-1-3084), the NSF (CBET 1911478), and the University of Washington for financial support. D.D. was supported by the China Scholarship Council.
Author contributions: D.D., C. Tsao, H.-C.H., and S.J. designed the study and interpreted the results. D.D., H.-C.H., and F.Y. developed and improved the protocols for the fabrication of hydrogels. D.D., H.-C.H., C. Tang, J. MacArthur, M.R.H., D.L., S.G.-h.T., and T.M.L. performed mechanical tests. D.D. and C. Tsao performed protein and cell adhesion tests. C. Tsao and L.N. performed hydrogel implantation. K.W., Priyesh Jain, and Parul Jain synthesized zwitterionic monomers. J. Ma, K.W., and F.Y. contributed to discussions on the results. D.D., C. Tsao, H.-C.H., A.S., and S.J. wrote the manuscript. All authors commented on the manuscript.
Competing interests: S.J. is a co-founder of Taproot Medical Technologies LLC. H.-C. H. and A.S. are employees of Taproot Medical Technologies LLC. S.J., H.-C.H., D.D., C. Tsao, C. Tang, and J. MacArthur are inventors on a pending patent related to this work filed by the University of Washington (PCT/US2019/046558 on 14 March 2019). All other authors declare that they have no competing interests. **Data and materials availability:** All data needed to evaluate the conclusions in the paper are present in the paper and/or the Supplementary Materials. Additional data related to this paper may be requested from the corresponding authors.

Submitted 5 May 2020
Accepted 6 November 2020
Published 1 January 2021
10.1126/sciadv.abc5442

Citation: D. Dong, C. Tsao, H.-C. Hung, F. Yao, C. Tang, L. Niu, J. Ma, J. MacArthur, A. Sinclair, K. Wu, P. Jain, M. R. Hansen, D. Ly, S. G.-h. Tang, T. M. Luu, P. Jain, S. Jiang, High-strength and fibrous capsule–resistant zwitterionic elastomers. *Sci. Adv.* **7**, eabc5442 (2021).